Insights into nitrobenzene adsorption mechanism on apricot stone activated carbon: A study via statistical physics models and thermodynamic analysis

Asma Mokhati, Zoubida Kecira, Oumessaâd Benturki, Maria Bernardo, Lotfi Sellaoui, Nesrine Mechi, Michael Badawi, Adrián Bonilla-Petriciolet

Insights into nitrobenzene adsorption mechanism on apricot stone activated carbon: A study via statistical physics models and thermodynamic analysis

Asma Mokhati [a,*], Zoubida Kecira [a], Oumessaâd Benturki [a], Maria Bernardo [b,*], Lotfi Sellaoui [c,d], Nesrine Mechi [c], Michael Badawi [e], Adrián Bonilla-Petriciolet [f]

[a] Laboratory of Physical and Chemical Study of Materials and Applications in the Environment, Faculty of Chemistry (USTHB), EL-Alia BP 32-16111, Algeria
[b] LAQV/REQUIMTE, NOVA School of Science and Technology, NOVA University Lisbon, Caparica 2829-516, Portugal
[c] Laboratory of Quantum and Statistical Physics, LR18ES18, Monastir University, Faculty of Sciences of Monastir, Tunisia
[d] CRMN, Centre for Research on Microelectronics and Nanotechnology of Sousse, NANOMISENE, LR16CRMN01, Sousse Code Postal 4054, Tunisia
[e] Université de Lorraine, CNRS, L2CM, Metz F-57000, France
[f] Instituto Tecnológico de Aguascalientes, Aguascalientes 20256, Mexico

GRAPHICAL ABSTRACT

- Apricot stones carbon used for nitrobenzene (NB) adsorption.
- Statistical physics models assess adsorption mechanism at micro and macro levels.
- Double layer adsorption model with two energies described NB adsorption mechanism.
- 2–3 adsorption sites involved in NB adsorption on carbon surface.
- Thermodynamics indicated exothermic, feasible and spontaneous removal of NB.

Keywords:
Water pollution
Activated carbon
Nitrobenzene
Double layer model

ABSTRACT

Statistical physics modelling was performed to analyze the adsorption forces and the thermodynamics of the removal of nitrobenzene molecules using an activated carbon obtained from apricot stones. This adsorbent was prepared using phosphoric acid activation and exhibited a surface area of 1762 $m^2\ g^{-1}$, total pore volume of 1.09 $cm^3\ g^{-1}$ and an experimental maximum adsorption capacity of 295.63 mg g^{-1} for nitrobenzene at 298 K. The removal of this organic molecule was exothermic. A double layer adsorption model with two energies was utilized to calculate the main steric parameters for the removal of this compound. This model was employed to perform a thermodynamic analysis of this adsorption system. It was concluded that 2 and 3 adsorption sites can be involved for the removal of nitrobenzene molecules on activated carbon surface. Physical interaction forces were expected to participate in the removal of this pollutant. This activated carbon can be regenerated with NaOH thus offering the alternative of its recycling to reduce the removal costs of this organic molecule from water.

* Corresponding authors.
E-mail addresses: amokhati@usthb.dz (A. Mokhati), maria.b@fct.unl.pt (M. Bernardo).

1. Introduction

The release of nitrobenzene (NB) compounds in the environment after the manufacturing of explosives, organic chemicals, and plastics generates pollution and serious risks to both human health and ecological systems even at trace concentrations [1,2]. This substance is considered a hazardous and toxic agent that is mutagenic and carcinogenic to humans [3,4]. It is characterized by its resistance to biodegradation thus being a long-term residue that accumulates into the environment [1]. In 2015, the United States Environmental Protection Agency (USEPA) categorized NB as a priority environmental pollutant and modified the permissible concentration of this substance from 17 to 10 μg L^{-1} in water, with the aim of protecting public health and the environment [5]. Therefore, several treatment technologies have been studied for the NB removal from water such as electrochemical methods [6,7], bioremediation [8,9], chemical oxidation [10,11], catalytic ozonation [12,13], and adsorption [14–16].

The adsorption employing biomass-derived activated carbons is a low-cost and effective method for NB removal from aqueous media [4, 17]. Nevertheless, the understanding of the adsorption mechanism (i.e., adsorbent-adsorbate and adsorbate-adsorbate interactions) that takes place for the removal of NB-related systems is crucial to improve the efficiency of this purification technology. The modeling of the adsorption equilibrium is a fundamental step in the characterization and comprehension of adsorption systems. Usually, empirical or semi-empirical models, such as Langmuir, Freundlich or Sips, are used to explain the adsorption phenomenon via the determination of some phenomenological parameters like the adsorption equilibrium constant [18]. However, these models lack the adsorption mechanism interpretation at the molecular scale [18–20]. For instance, the Langmuir model assumes that the adsorption takes place on a uniform (homogeneous) surface where the active sites exhibit similar energy and affinity with the adsorbate [21,22]. This model is inadequate to describe the interface of adsorbate—solid systems involving multi-interactions or multi-docking [22].

The advanced adsorption models based on the principles of statistical physics have been introduced to improve the explanation of the adsorption mechanisms. These models include physicochemical parameters that describe the steric and energetic factors linked to the interfacial phenomenon, i.e.: the number of molecules/ions adsorbed per active site (n), the density of adsorbent active sites (D), the adsorption capacity at saturation (Q_{sat}), and the adsorption energy (ΔE) [23–25]. These physicochemical parameters enable the explanation of adsorption mechanisms at both micro and macroscopic levels.

Statistical physics-based models were applied in the present work to obtain a new interpretation of the removal of NB molecules from water using an activated carbon. Different scenarios have been analyzed in the literature for the NB adsorption mechanism [1,2,4] where conventional adsorption models (e.g., Langmuir and Freundlich) have been applied to describe the interaction between the NB molecules and the activated carbon's surface. These previous studies were only focused on the analysis of the type of layers (mono- or multi-molecular layer) and the nature of the adsorbent surface (homogeneous or heterogeneous). Therefore, they provided an incomplete interpretation of the mechanism of NB adsorption at the molecular scale.

The primary goal of this study is to integrate experimental findings and data analysis derived from statistical physics models to elucidate the performance of a biomass-derived activated carbon for the removal of NB molecules from water at three different temperatures (298, 318, and 338 K). Stereographic and energetic physicochemical parameters from statistical physics models were employed to rationalize the adsorption mechanism of NB molecules at microscopic level. The application of these statistical physics-based adsorption models also facilitated the derivation, calculation, and interpretation of three thermodynamic functions: Entropy (S), Gibbs free energy (G), and Internal energy (E_{int}). These functions contributed to provide a detailed theoretical characterization of the NB adsorption process.

Overall, this study provides a novel perspective and in-depth insight of the interfacial interactions occurring between the NB molecule and the active sites of activated carbon at both micro- and macroscopic levels.

2. Materials and methods

2.1. Biomass feedstock for the activated carbon preparation – apricot stones

Apricot stones were used as feedstock to prepare the adsorbent and their processing was carried out according to a previous study [4]. The apricot kernels were washed, dried overnight at 110 °C, crushed, and then sieved to obtain particles ranging from 0.5 to 1.2 mm. These biomass particles were stored and utilized for the adsorbent preparation.

2.2. Synthesis and characterization of activated carbon

The biomass particles were impregnated with 85% phosphoric acid (H_3PO_4) by mass, using a biomass/H_3PO_4 mass ratio of 1/2 for 24 h at room temperature. The material obtained after the impregnation was carbonized employing a Carbolite 2416 tube furnace at 500 °C for 2 h with a heating rate 5 °C min^{-1} under the presence of nitrogen as inert gas stream. The carbonized sample was subjected to reflux with boiling water for 3 h. This step was followed by a further washing with boiling distilled water until a neutral pH was reached for the filtered water. The final activated carbon was dried in the oven at 110 °C for 24 h and then stored for its subsequent application.

The surface characteristics of the apricot-stone derived carbon (APS) were determined via N_2 adsorption/desorption isotherms obtained at 77 K with an ASAP 2010 Micromeritics equipment. The specific surface area (S_{BET}) was determined using BET method, the micropore volume (V_{Mic}) was obtained via the t-plot method, and the total pore volume (V_T) was measured via N_2 adsorption at a relative pressure of 0.95. On the other hand, the mesopore volume (V_{Mes}) was calculated by applying the formula: $V_{Mes} = V_T - V_{Mic}$, while the approximate average pore diameter (D_p)was determined using the next equation: $D_p = \frac{4V_T}{S_{BET}}$.

Fourier Transform Infrared Spectroscopy (FT-IR 4200 JASCO equipment) was utilized to analyze the chemical surface groups of the activated carbon sample using the KBr disk procedure. The determination of the pH of point of zero charge (pH_{PZC}) was performed following the methodology of Noh and Schwarz [26], where 0.15 g of the sample were mixed with 50 mL of 0.01 M NaCl solution. The pH range of the initial solutions ranged from 2.0 to 12.0 and this parameter was adjusted utilizing 0.1 M HCl and 0.1 M NaOH. The final pH of each solution was measured after 48 h of agitation and the pH_{PZC} value was determined from the plot of pH_{final} versus $pH_{initial}$.

2.3. Nitrobenzene adsorption studies

NB standard solution with a concentration of 1000 mg L^{-1} was prepared by dissolving an appropriate quantity of reactive grade NB (>99%, Biochim, Fluka, France) in ultrapure water. All the aqueous NB solutions with different concentrations were obtained via dilution of this standard solution. A summary of the main physicochemical characteristics of NB is presented in Table 1S (Supplementary Material).

The adsorption studies were conducted using the batch operation method, which involved adding 25 mg of APS sample to 25 mL of NB solution. The suspensions were agitated 24 h at a fixed temperature in a water bath orbital shaker. After the adsorption contact time, the suspensions were filtered and NB concentrations were quantified using UV-Vis spectrophotometry (Jasco equipment, model 630) at a maximum wavelength of 268.5 nm. The assessment of ASP adsorption properties to remove NB molecules was done via the calculation of adsorption ca-

pacity q_t (mg g^{-1}), which was determined using Eq. (1):

$$q_t = \frac{(C_i - C_f) \times V}{m} \quad (1)$$

Where C_i (mg L^{-1}) and C_f (mg L^{-1}) are the initial and final NB concentrations, V (L) is the solution volume and m (g) is the APS mass.

The pH impact on the NB removal was assessed by performing experiments with aqueous solutions with initial pH values from 2.0 to 12.0 and a contact time of 24 h. The kinetic study was performed measuring the NB adsorption capacities at different contact times from 5 to 480 min. The adsorption isotherm experiments were performed at 298, 318 and 333 K using initial NB concentrations varying from 20 to 200 mg L^{-1} and pH 6.5.

2.4. Nitrobenzene desorption studies

Regeneration cycles of APS were evaluated using H_2O and NaOH to desorb NB. In the initial phase, NB adsorption process was conducted as already described where 15 mg of APS were added to 25 mL of 100 mg L^{-1} NB solution in flasks. These flasks were agitated at 298 K until reaching the equilibrium. Finally, the NB-loaded adsorbent was separated by filtration from the solution and the pollutant concentrations were measured with UV–Vis spectroscopy. In the second phase of the regeneration experiment, NB-loaded adsorbent sample was mixed with 25 mL of the desorption medium (H_2O or 1 N NaOH). These suspensions were stirred with an orbital shaker in a water bath at 298 K for 4 h. Four regeneration cycles were carried out under identical operating conditions as detailed where all regenerated APS samples were washed and dried at 110 °C at each adsorption/desorption cycle. The removal efficiency (%) was used in the data analysis and calculated as follows:

$$Removal(\%) = \frac{(C_0 - C_f) \times 100}{C_0} \quad (2)$$

3. Results and discussion

3.1. APS characterization

N_2 adsorption–desorption isotherms of APS sample and its textural parameters are shown in Fig. 1. The isotherms of APS present a mix of type I and type IV, based on IUPAC classification [27]. An hysteresis loop was observed indicating the presence of mesopores [27,28]. The textural parameters of the APS sample indicated that it had a high surface area of 1762 m^2 g^{-1} with a high micropore volume (0.98 cm^3 g^{-1}) and low mesopore volume (0.11 cm^3 g^{-1}). The isotherms at lower pressures suggested that this adsorbent had a pore size distribution spanning a wide range, potentially encompassing broad micropores and narrow mesopores (< ~ 2.5 nm) [26]. In fact, the average pore diameter

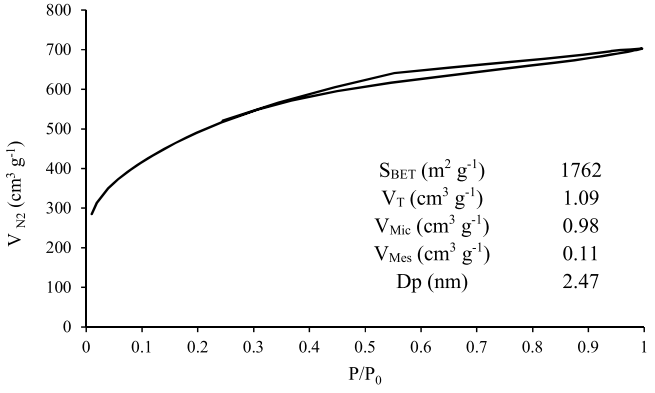

Fig. 1. N_2 adsorption-desorption isotherms at 77 K for APS sample and its textural parameters.

(D_p) value agreed with these characteristics.

Figure S1 (Supplementary material) shows that the pH_{PZC} value of APS was 4.3. Although this adsorbent was prepared using a H_3PO_4 activation, its surface had a low acidic character. Similar results were reported for argan nutshells activated with H_3PO_4 [27].

FTIR spectrum of APS is given in Fig. 2S (Supplementary material). The absorption bands at 3827, 3737, and 3637 cm^{-1} were attributed to the stretching elongations of alcohol groups (O-H). The asymmetric and symmetric C-H bonds were responsible for the less intense absorption bands identified at 2920 and 2850 cm^{-1}, respectively [4]. The absorption band located at 1680 cm^{-1} was attributed to (C═O) groups. The stretching vibration band located at 1384–1314 cm^{-1} was associated with the presence of methyl groups (–CH_3) [4]. The absorption band located at 1040 cm^{-1} could be attributed to the bending vibrations of P-O-P (phosphates groups) [29], which was related to the H_3PO_4 activation. The absorption bands identified at 924 and 674 cm^{-1} corresponded to the stretching deformation of C═C groups.

3.2. NB adsorption

3.2.1. pH and contact time effects

The effect of the solution pH on the NB removal using APS is reported in Fig. 3S (Supplementary material). These results indicated that solution pH changes had a limited impact on the adsorption of NB molecules onto APS surface. This finding was consistent with the characteristic of NB as a non-ionizable compound [30]. Therefore, the binding between NB molecules and APS surface might be driven primarily by hydrogen bonding, hydrophobic interactions, and/or π-stacking interactions [30]. Note that NB molecules have a weak acidic character due to the presence of the nitro group. As a result, the solution pH changes did not affect the ionization state of NB, which could impact the type of interactions of this molecule with activated carbon surfaces [4].

Fig. 4S (Supplementary material) illustrates the impact of contact time on the NB adsorption onto APS. The adsorption of this organic molecule was fast during within 60 min and reached the equilibrium after 180 min. The textural parameters of APS favored the mass transfer of NB molecules on internal pore structure. NB kinetic data were correlated with the pseudo-first order (PFO) and pseudo-second order (PSO) models [31]. RMSE (residual root means square error) and R^2 (determination coefficient) were used to compare the model performance:

$$RMSE = \sqrt{\frac{RSS}{m' - p}} \quad (3)$$

where RSS represents the residual sum of squares, which was determined by applying Eq. (4):

$$RSS = \sum_{j=1}^{m'} (q_{jexp} - q_{jcal})^2 \quad (4)$$

where q_{jexp} and q_{jcal} are the experimental and theoretical values of adsorbed NB amount, respectively, m' is the experimental data number, and p is the number of adjustable model parameters.

Table 2S (Supplementary material) shows the kinetic modelling results for NB adsorption. PSO provided the most accurate fit for NB-activated carbon system with R^2 = 0.994 and RMSE = 6.64. This model assumes that the adsorption occurs involving sharing or exchange electrons between adsorbate molecules and the adsorbent surface [31]. Typically, PFO and PSO models are employed to analyze the adsorption kinetic profiles. However, these models lack to elucidate the diffusivity mechanism and the rate-controlling processes responsible of the adsorbate removal [4]. For liquid-phase adsorption, the mass transfer of the adsorbate is frequently characterized by either film or intraparticle diffusion, or both [32]. The intraparticle diffusion model of Weber and Morris [31] can be utilized to analyze the NB kinetic profile with the aim

of identifying the mass transfer controlling step. This model is given by Eq. (5) as follows:

$$q_t = k_{id} \quad t^{1/2} + Z \tag{5}$$

Where k_{id} ($mg\,g^{-1}\,min^{-0,5}$) is the rate constant for intraparticle diffusion and Z ($mg\,g^{-1}$) is the constant related to the thickness of the boundary layer. The plot of $q_t$versus $t^{1/2}$ was used to correlate the NB kinetic data and the results are reported in Fig. 5S and Table 2S (Supplementary material). The intraparticle diffusion plot contained double linear segments indicating that the NB adsorption on APS was influenced by both film and intraparticle diffusion [33]. The results given in Table 2S (Supplementary material) indicated that the first regression line (film diffusion) showed the highest k_{id1} and lowest Z values, suggesting the rapid mass transfer of NB molecules into the APS porous structure, which was attributed to the presence of accessible and open pores. Note that the impact of the boundary layer (or external mass transfer) seemed to be relatively minor. The second regression line showed the lowest k_{id2} and the highest Z values, suggesting that the intraparticle diffusion process was relatively slow, which generated a significant concentration gradient of NB molecules.

3.2.2. NB adsorption equilibrium and theoretical explanation of the removal mechanism via statistical physics models

Fig. 2 shows the experimental isotherms of NB adsorption on APS at 298 – 338 K. An exothermic adsorption of this organic molecule was observed where the maximum experimental adsorption capacities ranged from 295.6 to 203.0 mg g^{-1} under tested operating conditions.

Three statistical physics models were applied to fit the isotherms of NB adsorption on APS. These models assumed the next scenarios: monolayer adsorption with a single energy (*Model 1*), monolayer adsorption with two adsorption energies (*Model 2*), and double layer adsorption with two energies (*Model 3*). The description and formulation of these models are given below.

Model 1: Monolayer adsorption with a single energy

Model 1 assumed that the NB molecules were adsorbed forming one layer on the APS surface with a contribution of one type of functional group participating in this process with a single interaction energy (i.e., Langmuir hypothesis) [34,35]. It was assumed that every functional group present on the APS surface had the capacity to adsorb a variable number of NB molecules, which differed of the well-established theory of the Langmuir model [34]. The expression of this model is given by Eq. (6):

$$q_e = \frac{nD_m}{1 + \left(\frac{C_{1/2}}{C_e}\right)^n} \tag{6}$$

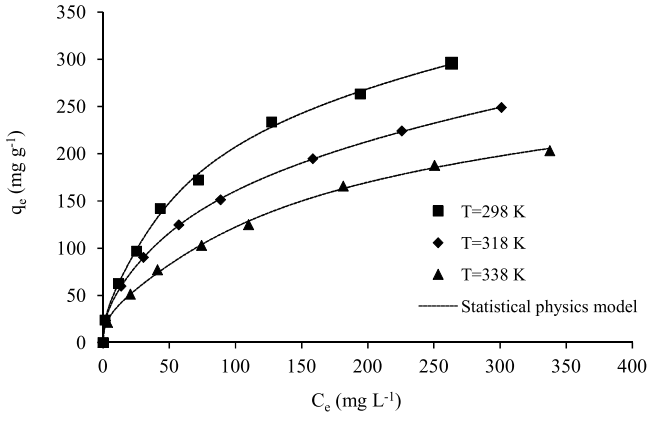

Fig. 2. Isotherms for the NB adsorption on APS and their modeling with statistical physics theory.

where n is the number of the NB molecules adsorbed per functional group (adsorption site) of APS surface, D_m (mgg^{-1}) is the density of adsorption sites at the saturation condition, and C_e and $C_{1/2}$ (mgL^{-1}) are the concentrations at equilibrium and half- saturation, respectively.

Model 2: Monolayer adsorption with two energies

This model assumed that the NB adsorption was a monolayer process involving two independent active sites where a specific quantity of NB molecules was anchored on site 1 with an adsorption site density D_1 and interaction energy $(-E_1)$, while the remaining NB molecules were attached to site 2 with an adsorption site density D_2 and an interaction energy $(-E_2)$ [36,37]. The expression of *Model 2* is defined by Eq. (7):

$$q_e = \frac{n_1 D_1}{1 + \left(\frac{C_1}{C_e}\right)^{n_1}} + \frac{n_2 D_2}{1 + \left(\frac{C_2}{C_e}\right)^{n_2}} \tag{7}$$

Where n_1 and n_2 represent the number of molecules adsorbed per first and second adsorption sites, respectively, while C_1 and C_2 (mgL^{-1}) are the concentrations at half saturation for these adsorption sites.

Model 3: Double layer adsorption with two energies

This model supposed that the adsorbed NB molecules could form two layers on the APS surface where two interaction energies were involved. The first energy $(-E_1)$ describes the interactions between the functionalities on the adsorbent surface and NB molecules, while the second energy $(-E_2)$ describes the interactions between the adsorbate molecules (i.e., NB – NB binding) [38]. *Model 3* is given by Eq. (8):

$$q_e = nD\frac{\left(\frac{C_e}{C_1}\right)^n + 2\left(\frac{C_e}{C_2}\right)^{2n}}{1 + \left(\frac{C_e}{C_1}\right)^n + \left(\frac{C_e}{C_2}\right)^{2n}} \tag{8}$$

A multivariable nonlinear regression analysis employing the Levenberg-Marquardt algorithm was utilized to fit these models to the experimental adsorption data. The best-fitted model was identified with R^2 and *RMSE* values besides the verification of reasonable trends for the calculated model parameters. The results of NB adsorption equilibrium modeling with three statistical physics models are reported in Table 1.

Overall, *Model 3* (double layer adsorption with two energies) provided the best description of the adsorption of NB molecules onto APS surface. Model 3 contains steric (n, D) and energetic (C_1, C_2) parameters that are useful to understand the adsorption mechanism at molecular scale [24]. The evolutions of these parameters are depicted in Fig. 2, while a detailed analysis is provided below.

a) *Steric parameters at APS saturation condition*

The stoichiometric coefficient n provides insights into the adsorption orientation (i.e., parallel or non-parallel) of the NB molecules on the APS. It is also applied to identify the aggregation phenomenon of the NB molecules on the aqueous solution [24,39,40]. Literature [18,34,41,42] indicates that the next scenarios can occur:

$n < 0.5$ indicates that the adsorbate molecule can interact via two

Table 1
Results of NB adsorption isotherm modeling using statistical physics equations.

R^2 for			
Temperature (K)	***Model 1***	***Model 2***	***Model 3***
298	0.9979	0.9979	0.9986
318	0.9998	0.9999	0.9999
338	0.9981	0.9997	0.9987
***RMSE* for**			
Temperature (K)	***Model 1***	***Model 2***	***Model 3***
298	4.60	4.60	3.72
318	1.07	3.40	0.54
338	2.99	2.99	2.45

or more adsorption sites (multi-interaction process).

$n < 1$ signifies a multi-anchorage process (or a parallel anchorage configuration) where the adsorbed molecule is attached parallel to the adsorbent surface with multiple anchor points.

$n > 1$ corresponds to the number of docked adsorbate molecules per adsorption site where the adsorption is multimolecular with each active site capable of simultaneously adsorbing various molecules. Note that the adsorbate molecules are expected to be anchored in a non-parallel position.

All the calculated n values for NB adsorption on APS were lower than 0.5, see Table 2. This result indicated that NB molecules adopted a parallel adsorption position on APS surface [43–45]. For tested temperatures, the n values can be derived as a weighted average from 0.30 to 0.50. The parameter $n' = 1/n$ can be defined as an anchorage number representing the number of occupied adsorption sites by a single molecule. It was observed that this anchorage number (n') was a nearly constant value around 2, thus indicating that NB molecule was docked into the activated carbon pores involving at least two adsorption sites [41].

The results of n values were used to estimate the percentages of molecules getting two anchorages ($n' = 2$) and three anchorages ($n' = 3$). If x represents the percentage of molecules with a single anchorage, and $(1 - x)$ is the percentage of molecules having dual anchorages. For instance, the value $n = 0.43$ can be obtained from a weighted mean between 0.3 and 0.5 and, consequently, Eq. (9) can be used:

$$0.43 = x \times 0.5 + (1 - x) \times 0.3 \quad (9)$$

Based on Eq. (9), it was inferred that 65% of the NB molecules were adsorbed with a double anchorage, while 35% corresponded to a triple anchoring.

Fig. 3 illustrates the calculated number of NB molecules adsorbed per active site and the receptor sites density versus temperature. The n parameter increased slightly from 0.427 to 0.432 with a temperature change from 298 to 318 K (Fig. 3a), then it decreased from 0.432 to 0.393 with a temperature increasing from 318 to 338 K. This trend could be explained by the change of interactions that resulted between NB molecules and the adsorption sites during the adsorption process. Same behavior was observed for SO_2 and NH_3 adsorption onto nanosheets composites (copper/graphene) [43].

Fig. 3b indicated that the trends of the number of NB molecules adsorbed per adsorption site and the adsorption site densities were different as the solution temperature changed. D parameter displayed two behaviors, it decreased from 102.5 mg g^{-1} at 298 K to 44.7 mg g^{-1} at 318 K and then it increased to 92.4 mg g^{-1} at 338 K. This decrease was attributed to the adsorption of NB molecules via multi-anchorages (i.e., tendency to aggregation) [46,47]. Note that around 35% of the nitrobenzene molecules were docked with triple adsorption sites. The increase of the occupied binding sites was associated to the decrease of the n parameter, leading to a reduction in a steric hindrance effect [40]. This behavior could be associated with alterations in the orientation of NB molecules on the carbon material resulting from the thermal agitation [48].

b) *Adsorption capacity at saturation*

The saturation adsorption capacity is fundamental to establish the maximum NB removal performance of APS. This parameter depended on solution temperature and pH, and it can be calculated using Eq. (10) [46]:

$$Q_{sat} = 2nD \quad (10)$$

Table 2 and Fig. 4 showed that the trend of Q_{sat} parameter had the same behavior of the adsorption site densities. Q_{sat} decreased from 298 to 318 K indicating a reduction in the ability of APS to bind NB molecules at the saturation state.

c) *Adsorption energies*

Adsorption energies were calculated to characterize the interactions of NB molecules and APS surface to form the two layers. They were

Table 2
Steric parameters calculated for NB adsorption on APS using Model 3.

Temperature (K)	*n*	*n' = 1/n*	*D (mg g^{-1})*	*Q_{sat} = 2 n*D (mg g^{-1})*
298	0.427	2.34	102.5	87.6
318	0.432	2.3	44.7	38.6
338	0.393	2.54	92.4	72.7

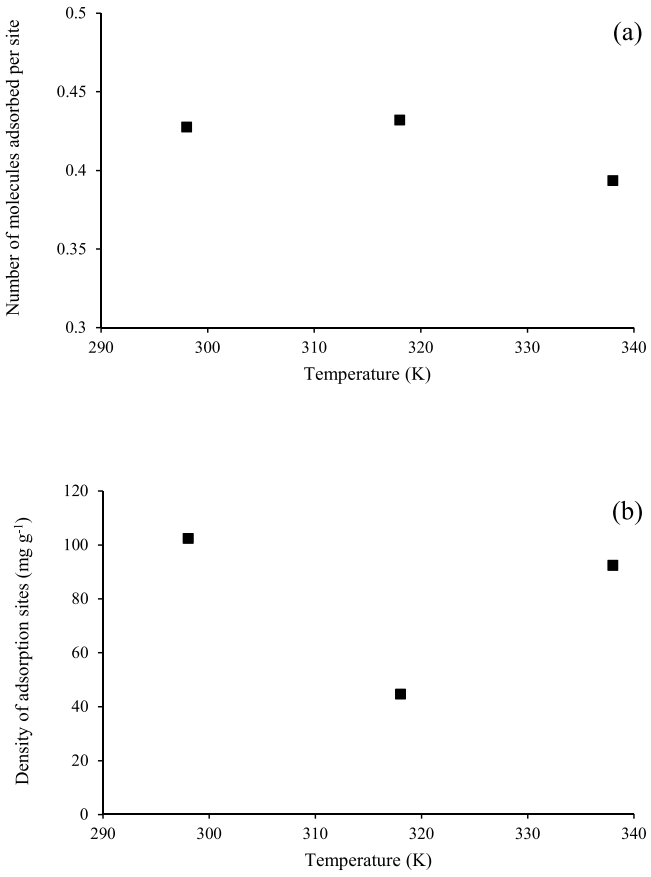

Fig. 3. (a) Calculated number of NB molecules adsorbed per adsorption site and (b) adsorption site densities of APS as a function of solution temperature.

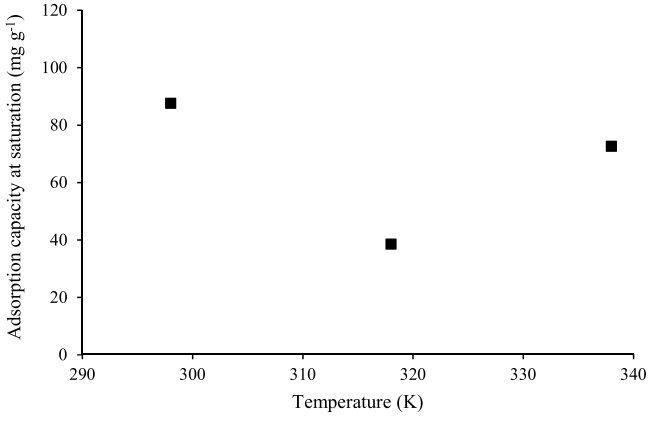

Fig. 4. Calculated Q_{sat} versus temperature for NB adsorption on APS.

obtained using Eqs. (11 and 12):

$$E_1 = RT\ln\left(\frac{C_s}{C_1}\right) \quad (11)$$

$$E_2 = RT\ln\left(\frac{C_s}{C_2}\right) \quad (12)$$

Where C_s represents the solubility of the nitrobenzene molecules ($mg\ L^{-1}$) in water at 298 K that was considered constant for tested three temperatures, R is the ideal gas constant ($R = 8.314\ J\ mol^{-1}\ K^{-1}$), and T is the absolute temperature (K). Calculated adsorption energies for NB adsorption are shown in Table 3 and Fig. 5. Contrary to the classical investigation, the results indicated that the absolute values of the first layer's adsorption energy at all temperatures were lower than the absolute values of adsorption energies of the second layer. Calculated adsorption energies were lower than 40 kJ/mol indicating that physisorption forces were responsible of the removal of NB molecules [49].

3.3. Thermodynamic functions for NB adsorption on APS

Three thermodynamic functions were calculated using the *Model 3* to elucidate the nature of the adsorption process of NB molecules on APS.

3.3.1. Entropy (S)

Entropy provides insights into the order and disorder of the adsorbate on the adsorbent surface [50]. The entropy expression based on *Model 3* as a function of the adsorbate equilibrium concentration is provided in Table 3S [51] (Supplementary material), while Fig. 6 shows this thermodynamic function versus NB concentration at tested temperatures.

It was observed that the entropy (S) varied increasing initially and then decreasing with an increase in NB concentration at all temperatures (Fig. 6). Calculated entropy values at 298 K were higher than those obtained for the other temperatures, which implied a greater disorder and molecular mobility within the system. This can be advantageous in the adsorption process as it allowed for more effective movement and interaction of adsorbate molecules with adsorbent surface, which was evidenced by the value of the saturation adsorption capacity at 298 K (Fig. 4). Adsorption entropy reached its maximum value near the second half-saturation concentration ($C_e = C_2$) indicating that system disorder was at its peak when NB molecules competed for the remaining vacant sites, where most of the adsorption sites were already occupied. For $C_e \geq C_2$, the number of vacant binding sites in the second layer decreased and the vacant states or positions for additional NB molecules became limited.

3.3.2. Gibbs free energy (G)

The Gibbs free energy expression using *Model 3* as a function of the adsorbate equilibrium concentration are given in Table 3S [51] (Supplementary material). Fig. 7 shows the calculated G versus NB concentration for NB removal. All the G values were negative, which proved that the nitrobenzene-APS adsorption system was thermodynamically spontaneous [22]. At 298 K, calculated G values exhibited more negative values, revealing a higher degree of spontaneity in the NB adsorption system and energetically favorable [51].

3.3.3. Internal energy (E_{int})

The internal energy E_{int} was calculated with *Model 3* using the equation reported in Table 3S [51] (Supplementary material) and the results are displayed in Fig. 8. At low concentration (i.e., $C_e \leq C_2$), calculated E_{int} values were positive indicating that NB-APS interactions were weaker than the interactions within the bulk phase of the NB molecules. Beyond the second half-saturation point ($C_e \geq C_2$), the calculated E_{int} values became negative showing that NB-APS interactions became stronger than at low concentration.

Table 3
Adsorption energies (E_1 and E_2) calculated for the NB removal on APS.

Temperature (K)	*C_1 (mg L^{-1})*	*C_2 (mg L^{-1})*	*E_1 (kJ mol^{-1})*	*E_2 (kJ mol^{-1})*
298	6.55	17.89	-2.83	-5.32
318	1.16	14.31	1.56	-5.09
338	10.60	35.88	-4.56	-7.99

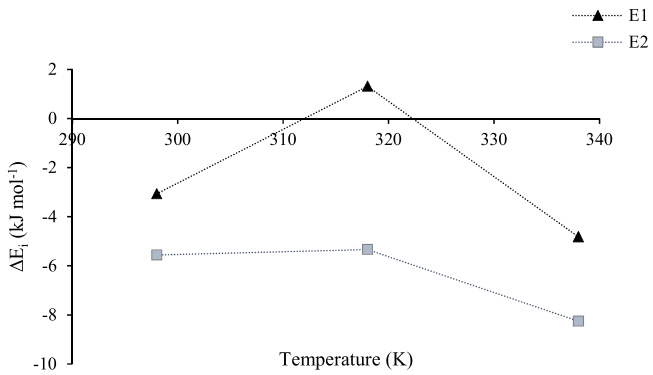

Fig. 5. Calculated adsorption energies *versus* temperature for the NB adsorption on APS.

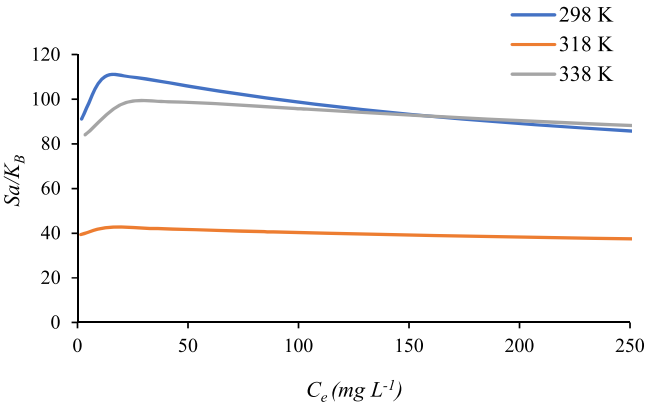

Fig. 6. Calculated entropy (S) for NB adsorption on APS at 298 – 338 K.

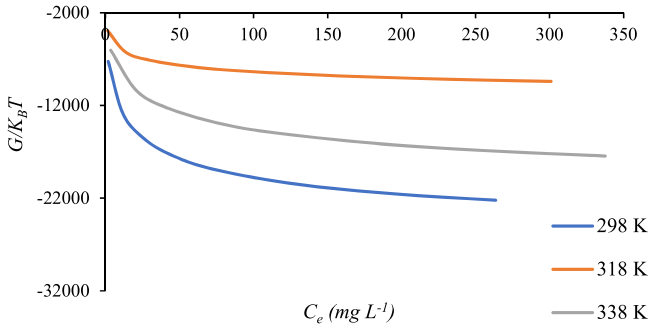

Fig. 7. Calculated Gibbs free energy (G) for NB adsorption on APS at 298–338 K.

3.4. Desorption studies

Fig. 6S (Supplementary material) reports the APS performance for different regeneration cycles. The results indicated that NB removal with APS reduced from 81% to 43% for H_2O and 81–60% for NaOH after four adsorption/desorption cycles. Therefore, NaOH is the best alternative to recover the adsorption properties of APS for NB removal.

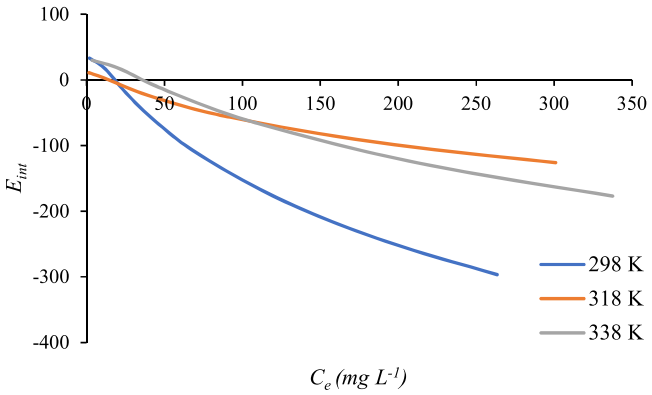

Fig. 8. Calculated internal energy (E_{int}) for NB adsorption on APS at 298 – 338 K.

4. Conclusions

The high specific surface area (1762 m^2 g^{-1}) and total pore volume (1.09 cm^3 g^{-1}) of the activated carbon derived from apricot stones make it an effective adsorbent for removing nitrobenzene molecules from water. The high adsorption capacity for nitrobenzene removal (295 mg g^{-1} at 298 K) of this activated carbon was attributed to their textural parameters. Statistical physics calculations indicated the existence of a double layer adsorption of nitrobenzene molecules on tested activated carbon, where two or three adsorption sites can be involved for binding one adsorbate molecule. The removal of this organic molecule was exothermic. Thermodynamic analysis of this adsorption process indicated a feasible and spontaneous process. Physical forces are expected to participate in the adsorption of nitrobenzene molecules on this activated carbon. Finally, this adsorbent can be regenerated using NaOH thus offering the possibility of its recycling to develop a low-cost water purification method.

CRediT authorship contribution statement

Michael Badawi: Writing – review & editing, Formal analysis. **Nesrine Mechi:** Writing – review & editing, Validation, Formal analysis. **Lotfi Sellaoui:** Writing – review & editing, Validation, Formal analysis. **Oumessaâd Benturki:** Writing – review & editing, Validation, Supervision, Resources, Funding acquisition. **Maria Bernardo:** Writing – review & editing, Visualization, Validation, Supervision, Formal analysis. **Zoubida Kecira:** Writing – original draft, Validation, Methodology, Investigation. **Asma Mokhati:** Writing – original draft, Visualization, Project administration, Methodology, Formal analysis, Conceptualization. **Adrián Bonilla-Petriciolet:** Writing – review & editing, Formal analysis.

Declaration of Competing Interest

The authors declare that they have no known competing financial interests or personal relationships that could have appeared to influence the work reported in this paper.

Data Availability

Data will be made available on request.

Acknowledgements

The authors would like to extend their gratitude for the financial assistance provided by the Faculty of Chemistry at USTHB, Algiers, and the Directorate General of Scientific Research and Technological Development (DGSRTD, Algiers). Maria Bernardo thanks FCT (Fundação para a Ciência e Tecnologia) for funding through program DL 57/2016 – Norma transitória.

Appendix A. Supporting information

Supplementary data associated with this article can be found in the online version at doi:10.1016/j.colsurfa.2024.133864.

References

[1] D. Wang, H. Shan, X. Sun, H. Zhang, Y. Wu, Removal of nitrobenzene from aqueous solution by adsorption onto carbonized sugarcane bagasse, Adsorpt. Sci. Technol. (2018), https://doi.org/10.1177/0263617418771823.
[2] W. Wei, R. Sun, J. Cui, Z. Wei, Removal of nitrobenzene from aqueous solution by adsorption on nanocrystalline hydroxyapatite, Desalination (2010), https://doi.org/10.1016/j.desal.2010.06.043.
[3] Safe Work Australia - Code of Practice, Safety data sheet: Nitrobenzene. (2006).
[4] Z. Kecira, O. Benturki, A. Benturki, M. Daoud, P. Girods, High adsorption capacity of nitrobenzene from aqueous solution using activated carbons prepared from vegetable waste, Environ. Prog. Sustain. Energy (2020), https://doi.org/10.1002/ep.13463.
[5] Office of Water U.S. Environmental Protection Agency Washington, Update of Human Health Ambient Water Quality Criteria: Nitrobenzene 98-95-3, USEPA, 2015.
[6] Z. Chen, Z. Wang, D. Wu, L. Ma, Electrochemical study of nitrobenzene reduction on galvanically replaced nanoscale Fe/Au particles, J. Hazard. Mater. (2011), https://doi.org/10.1016/j.jhazmat.2011.09.054.
[7] X. Zhao, A. Li, X. Quan, S. Chen, H. Yu, S. Zhang, Efficient electrochemical reduction of nitrobenzene by nitrogen doped porous carbon, Chemosphere (2020), https://doi.org/10.1016/j.chemosphere.2019.124636.
[8] R. Madadi, K. Bester, Fungi and biochar applications in bioremediation of organic micropollutants from aquatic media, Mar. Pollut. Bull. (2021), https://doi.org/10.1016/j.marpolbul.2021.112247.
[9] L. Cao, R. Ge, W. Xu, Y. Zhang, G. Li, X. Xia, F. Zhang, Simultaneous removal of nitrate, nitrobenzene and aniline from groundwater in a vertical baffled biofilm reactor, Chemosphere (2022), https://doi.org/10.1016/j.chemosphere.2022.136746.
[10] C. Tan, W. Yu, H. Mei, K. Chen, T. Xu, H. Xiang, Y. Feng, L. Deng, Simultaneous removal of nitrobenzene, benzoic acid, flunixin meglumine and aspirin by CaO2/Fe (III) system: Enhanced degradation by crystal boron, Sep. Purif. Technol. (2022), https://doi.org/10.1016/j.seppur.2022.122280.
[11] Y. Han, M. Qi, L. Zhang, Y. Sang, M. Liu, T. Zhao, J. Niu, S. Zhang, Degradation of nitrobenzene by synchronistic oxidation and reduction in an internal circulation microelectrolysis reactor, J. Hazard. Mater. (2019), https://doi.org/10.1016/j.jhazmat.2018.11.036.
[12] J. Hu, Y. Li, S. Nan, B.A. Yoza, Y. Li, Y. Zhan, Q. Wang, Q.X. Li, S. Guo, C. Chen, Catalytic ozonation of nitrobenzene by manganese-based Y zeolites, Front. Chem. (2020), https://doi.org/10.3389/fchem.2020.00080.
[13] P. Yan, J. Shen, L. Yuan, J. Kang, B. Wang, S. Zhao, Z. Chen, Catalytic ozonation by Si-doped A-Fe2O3 for the removal of nitrobenzene in aqueous solution, Sep. Purif. Technol. (2019), https://doi.org/10.1016/j.seppur.2019.115766.
[14] J. Li, C. Sun, C. Wen, L. Wang, Y. Zhao, W. Li, Z. Chang, A stable multifunctional Zn (II) based metal-organic framework for sensitive detection of Hg(II), Cr(VI), nitrobenzene and adsorption of methylene blue, J. Environ. Chem. Eng. (2022), https://doi.org/10.1016/j.jece.2022.107880.
[15] X. Li, X. Zhang, Y. Xu, P. Yu, Removal of nitrobenzene from aqueous solution by using modified magnetic diatomite, Sep. Purif. Technol. (2020), https://doi.org/10.1016/j.seppur.2020.116792.
[16] G. Lee, G. Park, S. Kim, S.H. Jhung, Adsorptive removal of aromatic diamines from water using metal-organic frameworks functionalized with a nitro group, J. Hazard. Mater. (2023), https://doi.org/10.1016/j.jhazmat.2022.130133.
[17] Y. Dai, D. Zhang, K. Zhang, Nitrobenzene-adsorption capacity of NaOH-modified spent coffee ground from aqueous solution, J. Taiwan Inst. Chem. Eng. (2016), https://doi.org/10.1016/j.jtice.2016.08.042.
[18] C. Yanan, Z. Srour, J. Ali, S. Guo, S. Taamalli, V. Fèvre-Nollet, K. da Boit Martinello, J. Georgin, D.S.P. Franco, L.F.O. Silva, G.L. Dotto, A. Erto, F. Louis, A. El Bakali, L. Sellaoui, Adsorption of paracetamol and ketoprofenon activated charcoal prepared from the residue of the fruit of Butiacapitate: experiments and theoretical interpretations, Chem. Eng. J. (2023), https://doi.org/10.1016/j.cej.2022.139943.
[19] L. Sellaoui, S. Knani, A. Erto, M.A. Hachicha, A. Ben Lamine, Equilibrium isotherm simulation of tetrachlorethylene on activated carbon using the double layer model with two energies: steric and energetic interpretations, Fluid Phase Equilibria (2016), https://doi.org/10.1016/j.fluid.2015.09.022.
[20] L. Sellaoui, L.F.O. Silva, M. Badawi, J. Ali, N. Favarin, G.L. Dotto, A. Erto, Z. Chen, Adsorption of ketoprofen and 2- nitrophenol on activated carbon prepared from winery wastes: a combined experimental and theoretical study, J. Mol. Liq. (2021), https://doi.org/10.1016/j.molliq.2021.115906.
[21] I. Langmuir, The constitution and fundamental properties of solids and liquids. II. Liquids. J. Am. Chem. Soc. (1917) https://doi.org/10.1021/ja02254a006.
[22] I.A. Ahmed, M. Badawi, A. Bonilla-Petriciolet, E.C. Lima, M.K. Seliem, M. Mobarak, Insights Into the Mn(VII) and Cr(VI) adsorption mechanisms on purified diatomite/

MCM-41 composite: experimental study and statistical physics analysis, Front. Chem. (2022), https://doi.org/10.3389/fchem.2021.814431.
[23] S. Wjihi, C. Briki, L. Sellaoui, A. Jemni, A. Ben Lamine, Theoretical study of hydrogen desorption on Mg50Ni50 using statistical physics treatment, Int. J. Hydrog. Energy (2017), https://doi.org/10.1016/j.ijhydene.2016.07.114.
[24] Sellaoui L., Saha B.B., Wjihi S., Ben Lamine A. Physicochemical parameters interpretation for adsorption equilibrium of ethanol on metal organic framework: Application of the multilayer model with saturation. Journal of Molecular Liquids, https://doi.org/10.1016/j.molliq.2016.07.017.
[25] T. Altalhi, G. Jethave, U. Fegade, G.A.M. Mersal, M.M. Ibrahim, M.H.H. Mahmoud, T. Kumeria, K.A. Isai, M. Sonawane, Adsorption of magenta dye on PbO Doped MgZnO: interpretation of statistical physics parameters using double-layer models, Int. J. Environ. Res. Public Health (2022), https://doi.org/10.3390/ijerph191912199.
[26] J.S. Noh, J.A. Schwarz, Estimation of the point of zero charge of simple oxides by mass titration, J. Colloid Interface Sci. (1989), https://doi.org/10.1016/0021-9797(89)90086-6.
[27] Thommes M., Kaneko K., V Neimark A., Olivier J.P., Rodriguez-reinoso F., Rouquerol J., Sing K.S.W. (2015). Physisorption of gases, with special reference to the evaluation of surface area and pore size distribution. IUPAC Technical Report, https://doi.org/10.1515/pac-2014-1117.
[28] A. Mokhati, O. Benturki, Z. Kecira, M. Bernardo, I. Matos, N. Lapa, M. Ventura, O.S. G.P. Soares, A.M.B. do Rego, I.M. Fonseca, Nanoporous carbons prepared from argan nutshells as potential removal agents of diclofenac and paroxetine, J. Mol. Liq. (2021), https://doi.org/10.1016/j.molliq.2021.115368.
[29] J. Coates, Interpretation of infrared spectra, a practical approach, Encycl. Anal. Chem. (2006), https://doi.org/10.1002/9780470027318.a5606.
[30] Q. Qin, J. Ma, K. Liu, Adsorption of nitrobenzene from aqueous solution by MCM-41, J. Colloid Interface Sci. (2007), https://doi.org/10.1016/j.jcis.2007.06.060.
[31] Y. HO, Review of second-order models for adsorption systems, J. Hazard. Mater. (2006), https://doi.org/10.1016/j.jhazmat.2005.12.043.
[32] C. Yao, T. Chen, A film-diffusion-based adsorption kinetic equation and its application, Chem. Eng. Res. Des. (2017), https://doi.org/10.1016/j.cherd.2017.01.004.
[33] B. An, Cu(II) and As(V) adsorption kinetic characteristic of the multifunctional amino groups in chitosan, Processes (2020), https://doi.org/10.3390/PR8091194.
[34] M. Touihri, F. Guesmi, C. Hannachi, B. Hamrouni, L. Sellaoui, M. Badawi, J. Poch, N. Fiol, Single and simultaneous adsorption of Cr(VI) and Cu (II) on a novel Fe3O4/pine cones gel beads nanocomposite: experiments, characterization and isotherms modeling, Chem. Eng. J. (2021), https://doi.org/10.1016/j.cej.2021.129101.
[35] A. Gómez-Avilés, L. Sellaoui, M. Badawi, A. Bonilla-Petriciolet, J. Bedia, C. Belver, Simultaneous adsorption of acetaminophen, diclofenac and tetracycline by organo-sepiolite: experiments and statistical physics modelling, Chem. Eng. J. (2021), https://doi.org/10.1016/j.cej.2020.126601.
[36] S. Knani, M. Mathlouthi, A. Ben Lamine, Modeling of the psychophysical response curves using the grand canonical ensemble in statistical physics, Food Biophys. (2007), https://doi.org/10.1007/s11483-007-9042-7.
[37] G.L. Dotto, L. Sellaoui, E.C. Lima, A. Ben Lamine, Physicochemical and thermodynamic investigation of Ni(II) biosorption on various materials using the statistical physics modeling, J. Mol. Liq. (2016), https://doi.org/10.1016/j.molliq.2016.04.075.
[38] L. Sellaoui, A. Gómez-Avilés, F. Dhaouadi, J. Bedia, A. Bonilla-Petriciolet, S. Rtimi, C. Belver, Adsorption of emerging pollutants on lignin-based activated carbon: analysis of adsorption mechanism via characterization, kinetics and equilibrium studies, Chem. Eng. J. (2023), https://doi.org/10.1016/j.cej.2022.139399.
[39] L. Sellaoui, D.S.P. Franco, G.L. Dotto, É.C. Lima, A. Ben Lamine, Single and binary adsorption of cobalt and methylene blue on modified chitin: application of the Hill and exclusive extended Hill models, J. Mol. Liq. (2017), https://doi.org/10.1016/j.molliq.2016.10.079.
[40] S. Wjihi, F. Aouaini, A.H. Almuqrin, A. Ben Lamine, Physicochemical assessment of prednisone adsorption on two molecular composites using statistical physics formalism in cosmetics, Arab. J. Chem. (2020), https://doi.org/10.1016/j.arabjc.2020.06.040.
[41] L. Sellaoui, H. Guedidi, S. Masson, L. Reinert, J.M. Levêque, S. Knani, A. Ben Lamine, M. Khalfaoui, L. Duclaux, Steric and energetic interpretations of the equilibrium adsorption of two new pyridinium ionic liquids and ibuprofen on a microporous activated carbon cloth: Statistical and COSMO-RS models, Fluid Phase Equilibria (2016), https://doi.org/10.1016/j.fluid.2016.01.007.
[42] M.S. Shamsudin, S.F. Azha, L. Sellaoui, M. Badawi, Y. Alghamdi, A. Bonilla-Petriciolet, S. Ismail, Fabrication and characterization of a thin coated adsorbent for antibiotic and analgesic adsorption: experimental investigation and statistical physical modelling, Chem. Eng. J. (2020), https://doi.org/10.1016/j.cej.2020.126007.
[43] L. Zhang, L. Yang, J. Chen, X. Zhou, Adsorption of SO2 and NH3 onto copper/graphene nanosheets composites: statistical physics interpretations, thermodynamic investigations, and site energy distribution analyses, Chem. Eng. J. (2022), https://doi.org/10.1016/j.cej.2022.137224.
[44] I. Ben Khemis, N. Mechi, L. Sellaoui, A. Ben Lamine, Modeling of muscone enantiomers olfactory response by an adsorption process onto the mouse muscone receptor MOR215-1, J. Mol. Liq. (2016), https://doi.org/10.1016/j.molliq.2016.06.021.
[45] L. Sellaoui, A. Yazidi, S. Taamalli, A. Bonilla-Petriciolet, F. Louis, A. El Bakali, M. Badawi, E.C. Lima, D.R. Lima, Z. Chen, Adsorption of 3-aminophenol and resorcinol on avocado seed activated carbon: mathematical modelling, thermodynamic study and description of adsorbent performance, J. Mol. Liq. (2021), https://doi.org/10.1016/j.molliq.2021.116952.
[46] M. Khalfaoui, M.H.V. Baouab, R. Gauthier, A. Ben Lamine, Statistical physics modelling of dye adsorption on modified cotton, Adsorpt. Sci. Technol. (2002), https://doi.org/10.1260/026361702760120908.
[47] C. Djama, A. Bouguettoucha, D. Chebli, A. Amrane, H. Tahraoui, J. Zhang, L. Mouni, Experimental and theoretical study of methylene blue adsorption on a new raw material, cynara scolymus—a statistical physics assessment, Sustainability (2023), https://doi.org/10.3390/su151310364.
[48] E. Allahkarami, A. Dehghan Monfared, L.F.O. Silva, G.L. Dotto, Toward a mechanistic understanding of adsorption behavior of phenol onto a novel activated carbon composite, Sci. Rep. (2023), https://doi.org/10.1038/s41598-023-27507-5.
[49] B. Cheknane, F. Zermane, O. Bouras, J. Debord, M. Harel, J.C. Bollinger, L. Sellaoui, A. Bonilla-Petriciolet, Modeling of binary and ternary batch adsorption systems via multidimensional logistic distribution and statistical physics, J. Environ. Chem. Eng. (2021), https://doi.org/10.1016/j.jece.2021.105664.
[50] L. Sellaoui, T. Depci, A.R. Kul, S. Knani, A. Ben Lamine, A new statistical physics model to interpret the binary adsorption isotherms of lead and zinc on activated carbon, J. Mol. Liq. (2016), https://doi.org/10.1016/j.molliq.2015.12.080.
[51] L. Zhang, L. Yang, J. Chen, W. Yin, Y. Zhang, X. Zhou, F. Gao, J. Zhao, Adsorption of Congo red and methylene blue onto nanopore-structured ashitaba waste and walnut shell-based activated carbons: statistical thermodynamic investigations, pore size and site energy distribution studies, Nanomaterials (2022), https://doi.org/10.3390/nano12213831.